UAV AUTOMATIC LANDING ON A SHIP-DECK, MULTIVARIATE SENSOR FUSION FOR ROBUST STATE ESTIMATION

Antonio Digiacomo, Leonardo Helicopters, Cascina Costa (VA), Italy
Matteo Baiguera, Leonardo Helicopters, Cascina Costa (VA), Italy

Abstract

In response to the growing demand for autonomy and reliability of Uncrewed Aerial Vehicles (UAV), this research presents a navigation solution for the automatic landing of an uncrewed rotorcraft on a ship-deck based on computer vision enhanced through sensor fusion with data from the attitude heading reference system (AHRS) and radio beacons. Conducted by a team of Leonardo Helicopter Division, this study addresses the case of a GPS or data-link loss and includes the creation of a relative pose estimation algorithm based on the detection of Fiducial Markers, complemented by the formulation of an Unscented Kalman Filter (UKF) and sensor modeling based on test data. Results are obtained in a simulation environment relying on ROS 2 (Robot Operative System 2) for inter-process communication, Ansys® AVxcelerate for optical sensor and environment modeling, and a proprietary software responsible for guidance, control logics, and dynamics simulation. Research findings showcase promising outcomes and open avenues for future enhancements, including real-world testing.

1. NOTATION

Mathematical formulations in this paper contain variables that can be referred to both different vehicles and different reference frames. For this reason, some variables contain two subscripts defining the vehicle they refer to and the coordinate system they are expressed in. Below is the list of symbols associated with physical and statistical values.

Symbols

- P State covariance matrix
- Q Process noise covariance matrix
- R Measurement noise covariance matrix
- u Kalman filter input vector
- x Kalman filter state vector
- z Measurement vector
- α Elevation angle, rad
- γ Azimuth angle, rad
- φ Roll angle, rad
- θ Pitch angle, rad
- ψ Yaw angle, rad
- x_{ij} Position vector of j with respect to i frame, m
- R_{ij} Rotation matrix from i frame to j frame
- V_{ij} Velocity vector of j relative to i in i frame, m/s
- ω_{ij} Angular body velocity vector of j in i frame, rad/s

The list below shows the symbols identifying the four reference frames that are used as subscripts to define physical variables.

Reference frames identifiers

- C Camera reference frame, oriented as in the Pinhole camera model
- H UAV body frame
- T Touch down point (TDP) body frame, oriented as the ship body frame
- W World: inertial coordinate system oriented as the North-East-Down system

1. INTRODUCTION

In recent years, GNSS-denied navigation in maritime environments has gained significant attention due to the increasing need of having a system that does not fully rely on GPS data, which may be compromised by jamming or spoofing events or undergo degraded performance under adversarial conditions at low altitude (Ref. 1).

The considered scenario for this research is that of an uncrewed rotorcraft subjected to a GPS or data-link loss during the navigation towards the landing site on a ship-deck. This study focuses on the ship-UAV relative state estimation during the final part of the approach and tackles the problem of obtaining sufficiently accurate information regarding the two vehicles to allow for an autonomous landing. Figure 1 shows the coordinate systems involved in the formulation of the problem.

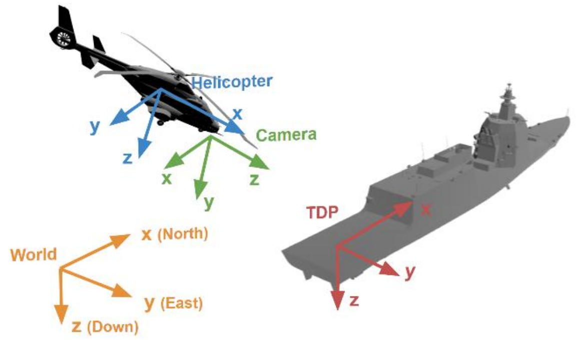

Figure 1: coordinate systems.

Fiducial markers offer a highly distinguishable pattern with strong visual characteristic (Ref. 2) and represent an optimal way to carry out a fast, simple, and robust relative pose estimation between the UAV and the touchdown point (TDP) using a camera and computer vision methods. In addition, the development of a sensor fusion algorithm allows to integrate other data sources, such as the AHRS and Radio beacons, to broaden the relative state information, enhance the pose estimation accuracy, and provide a kinematic model to propagate the state when sensor data is missing.
A significant amount of research has been conducted in the use of vision and sensor fusion algorithms for deck landing (Refs. 3, 4, 5), yet a considerable challenge persists in devising a safe solution to be deployed, tested, and integrated with real hardware.

This research presents the development of a vision-based navigation solution, integrated in the flight control system (FCS) and dynamics simulation software, where processed and simulated sensor data merge into an Unscented Kalman Filter (UKF) for state estimation.

The proprietary FCS model, developed in Simulink, includes the real on-board flight control computer (FCC) software, apart from sensors, actuators, engine, and dynamics simulations. It communicates with the navigation system, sending ground truth and AHRS data and receiving the relative state estimation. As shown in Figure 2, the true UAV and ship poses are utilized to generate camera images and to compute the simulated radio beacons' directions of arrival (DOA) estimation. Sensor data is processed by the UKF that sends the relative state estimation back to the FCS software.

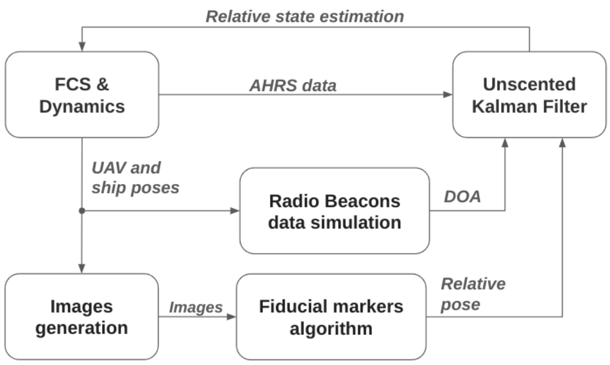

Figure 2: Simulation loop scheme.

2. SIL AND SIMULATION TOOLS

2.1. Renderer

The proposed simulation solution for replicating optical sensor output relies on Ansys AVxcelerate® (Ref. 6). Ansys' software distinguishes itself by its capacity to simulate diverse atmospheric conditions such as sunlight, snow, rain, and fog across different times of the day. Such environmental representation ensures a holistic and realistic testing environment for prototypes (Ref. 7).

Moreover, via a dedicated tool, AVxcelerate® allows to model physical sensors by assigning properties that are a one-to-one match with sensor datasheets, like lenses properties, coating materials, and post-processing imager characteristics for a camera.

Crucial for this work is the simulator's capability to provide real-time positional information for all simulated objects relative to the world's origin, that is, the zero-coordinate point, set by the simulator, from which the entire position vector and rotation angles are calculated.

To ensure syncing between all processes involved (e.g., between the sensor rendering and the helicopter and ship poses), AVxcelerate® has been interfaced to a widely diffused robotic middleware (ROS2) (Refs. 8, 9), allowing a rapid development of the perception pipeline presented here, heading to a full SIL capability.

From a mere software perspective, all Access Programming Interfaces (APIs) exposed by the Ansys simulation tool have been wrapped in three types of ROS2 nodes:

- *AVx-Trajectory-Commander*: responsible for commanding agents poses at real time in the simulation.
- *AVx-Data-Manager*: responsible for streaming in the ROS2 network the sensor output. To minimize communication latency, the shared memory communication protocol has been identified for retrieving raw sensor data from the simulator, while the gRPC protocol is instead used to notify when a new sensor data is available.
- *AVx-Updater*: "master" node commanding a new simulation step, updating all agents poses only after the sensor data generation and communication has been finalized.

An explanatory scheme of the software architecture is depicted in Figure 3.

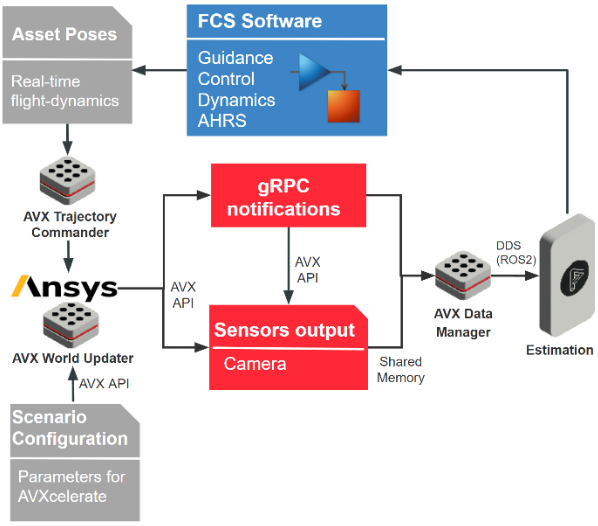

Figure 3: software architecture.

2.2. FCS - SW loop interconnection

In order to assess control performances of the H/c under the approximated ship deck pose estimation provided by the sensor fusion approach presented here, the H/c flight dynamics system model have been connected to the ROS2 stack and therefore synced with the sensor simulator, via a dedicated UDP socket. This model has been implemented in past years in the context of unmanned Leonardo® and it is available to authors in the form of a Simulink diagram with a dedicated block including the actual on-board software of the UAV.

The nominal approaching trajectory, shown in Figure 4, is also computed by the above-mentioned diagram where landing trajectory waypoints are set in the initialization step prior to the actual start of the simulation.

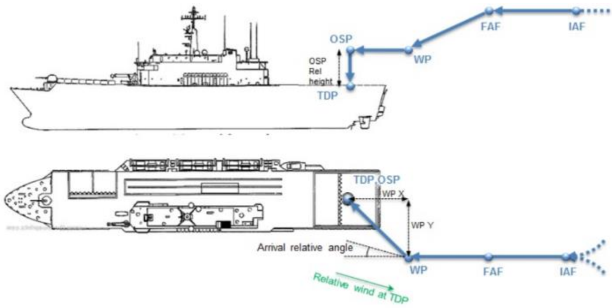

Figure 4: Nominal trajectory and relative waypoints for ship deck approach.

3. SENSORS SETUP

3.1. Pinhole camera and fiducial markers

Camera images are crucial for the navigation setup under consideration, as they are processed by a computer vision algorithm to detect a board of four fiducial markers placed on the wall in front of the ship-deck, as shown in Figure 5.

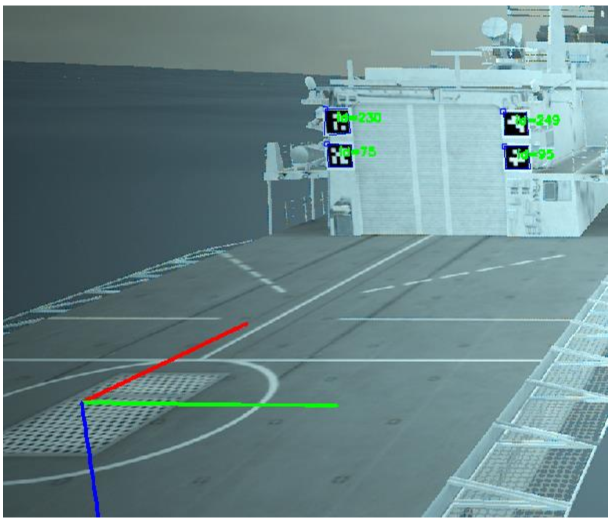

Figure 5: Fiducial markers detection and TDP frame pose estimation.

The goal of the detection process is to identify the corners and the corresponding ID number of each detected marker. Then the information about the pixel coordinates of the corners is combined with the prior knowledge of their corresponding real 3D coordinates relative to the TDP to solve the Perspective-n-Point problem (Ref. 10). The final output consists of the position and the orientation of the TDP with respect to the camera frame, oriented according to the Pinhole model as shown in Figure 1.

The presence of an additional white border around the markers helps the detection algorithm perform the segmentation using a local adaptive method (Ref. 11). The use of a board of markers guarantees a significantly better performance compared to that of single markers for the following reasons:

- It allows for a more continues estimation: if a marker is undetected the estimation can still be carried out with the other ones.
- The PnP problem can be solved using a wider set of points, increasing the precision.
- The distribution of detected marker corners covers a wide region of space; thus, the pose estimation performance improves.

Geometric data about the fiducial markers' setup is shown in Table 2.

Table 2: Fiducial markers setup, geometric data.

Parameter	Value
Markers' width	1.2 m
Horizontal distance	7.3 m
Vertical distance	1.4 m

Once the TDP frame position and orientation with respect to the camera have been determined, Eq. 1 and Eq. 2 are applied to transform the computed pose and make it relative to the UAV frame.

(1) $$\boldsymbol{x}_{HT} = \boldsymbol{x}_{HC} + \boldsymbol{R}_{HC}\boldsymbol{x}_{CT}$$

(2) $$\boldsymbol{R}_{HT} = \boldsymbol{R}_{HC}\boldsymbol{R}_{CT}$$

The rotation matrix in Eq. 2 is then turned into Euler angles to obtain the final output of the fiducial markers algorithm as shown in Eq. 3.

(3) $$\boldsymbol{z}_{markers} = [\boldsymbol{x}_{HT}^{\top}, \boldsymbol{\Omega}_{HT}^{\top}]^{\top}$$

Table 2 shows the parameters of the simulated camera.

Table 2: camera parameters.

Parameter	Value
Focal length	10.00 mm
Sensor width	20.30 mm
Sensor height	11.25 mm
Resolution width	1920 pixels
Resolution height	1080 pixels

With the presented camera parameters, the first detection occurs at about 40 meters from the touchdown point. A bigger focal length - thus a narrower field of view (FOV) - would allow for a more distant detection. However, as discussed in Ref. 12, a large FOV is a safer choice, as it lowers the probability that the UAV loses the view of markers during the landing.

3.2. Radio Beacons

Radio Beacons system provides additional information regarding the relative state between UAV and ship. It is made of the following components:

- Onboard receiver (RX), placed on the drone, inclined downwards of 30 degrees.
- Three transmitters (TX) placed on the ship deck in the vertices of an equilateral triangle centered on the TDP.
- A companion board in the UAV that elaborates the sensor information from the received signals.

The position estimation of the UAV is achieved through a process of time-based localization. Signals time-of-flight, combined with relative range information from the Received Signal Strength Indicator (RSSI), offers a means to triangulate the UAV position in Cartesian coordinates.

With the purpose of including radio beacons in the simulation, suppliers provided test data about the accuracy of the system in the form of mean square error (MSE) as a function of the relative position coordinates between transmitter and receiver. Data is stored in a MATLAB file containing three-dimensional arrays where each element represents the MSE corresponding to a defined x-y-z coordinate. Figure 6 shows how MSE data looks when displayed on a 3D graph, considering a fixed relative height.

Position estimation retrieved from radio beacons companion board has a much higher noise compared to that of fiducial markers estimations, thus it does not bring a relevant improvement when it fused in the UKF. However, radio beacons also provide accurate measurements of the directions of arrival corresponding to the azimuth and elevation of the UAV relative to the TDP.

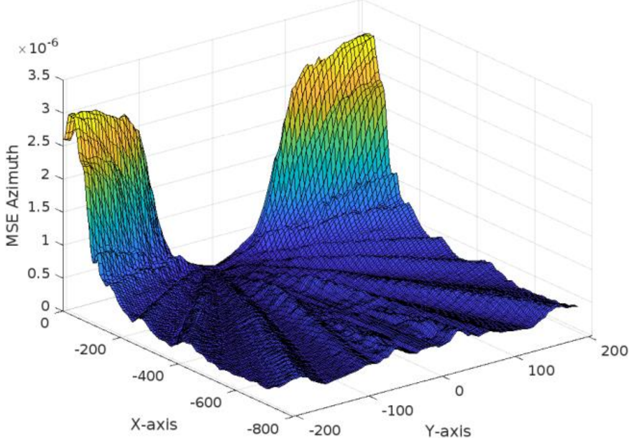

Figure 6: MSE of Azimuth beacons estimation as a function of the distance from the TDP on a horizontal plane at fixed altitude (65 m).

Along with fiducial markers data, the measurement shown in Eq. 4 is used to update the UKF state estimations.

$$\boldsymbol{z}_{beacons} = [\gamma, \alpha]^\top \tag{4}$$

To simulate beacons data, ground truth vehicles' poses are employed to derive the relative position and find the corresponding MSE. This is utilized to generate a random gaussian error that is then added to the true azimuth and elevation, calculated as shown in Eq. 5, 6.

$$\gamma = \arccos\left(-\frac{y_{TH}}{\sqrt{x_{TH}^2+y_{TH}^2}}\right) \tag{5}$$

$$\alpha = \arcsin\left(-\frac{z_{TH}}{\sqrt{x_{TH}^2+y_{TH}^2+z_{TH}^2}}\right) \tag{6}$$

The UAV position relative to the TDP frame is computed as in Eq. 7.

$$\boldsymbol{x}_{TH} = \boldsymbol{R}_{WT}^\top(\boldsymbol{x}_{WH} - \boldsymbol{x}_{WT}) \tag{7}$$

3.3. Attitude Heading Reference System

The Attitude Heading Reference System (AHRS) consists of a set of sensors such as three-axis gyroscopes, accelerometers, and magnetometers that measure angular body rates and inertial accelerations and provide information on the attitudes of the vehicle. The AHRS of the UAV considered in this research has a fiber-optic gyroscope (FoG). which have and exceptionally low bias instability, with an angular drift close to zero for a period up to one or two hours. On the other hand, the loss of GPS signal affects in a considerable way both velocity and position because of the integration of linear accelerations. Eq. 8 shows the AHRS data which is used as input vector for the propagation model of the UKF.

$$\boldsymbol{u}_{AHRS} = [\boldsymbol{\Omega}_{WH}^\top, \boldsymbol{V}_{WH}^\top, \boldsymbol{\omega}_{HH}^\top]^\top \tag{8}$$

To simulate the performance degradation after the GPS loss, a linear drift in velocities is added, based on data provided by the AHRS supplier, as shown in table 3.

Table 3: AHRS drift performance

Time	Velocity Drift
5 minutes	< 1 m/s
30 minutes	< 3 m/s
60 minutes	< 4 m/s

Drift in linear velocities causes a considerable divergence of position estimation. However, in the final part of the approach, the FCS employs the relative state as input to the control. In particular, the control system requires relative North-East-Up (NEU) position and velocities to make the rotorcraft navigate towards the touchdown point.

4. UKF FORMULATION

4.1. Overview and fundamentals

The purpose of using a Kalman Filter is estimating the state of the system $\boldsymbol{x}$ and its covariance $\boldsymbol{P}$ by combining pieces of information coming from sensors and a mathematical formulation. The filter model is composed by the state transition function f, to propagate the state and predict its evolution in time, and the measurement function h, that links the state to the observations. For each time step k, the system of equations described in Eq. 9 defines the evolution of the state and observed variables.

$$\begin{gathered} \boldsymbol{x}_k = f(\boldsymbol{x}_{k-1}, \boldsymbol{u}_k) \\ \boldsymbol{z}_k = h(\boldsymbol{x}_k) \end{gathered} \tag{9}$$

Predictions and measurement are respectively affected by process noise (v) and measurement noise (w), assumed as zero-mean Gaussian noises, and their statistics is defined by covariance matrices $\boldsymbol{Q}$ and $\boldsymbol{R}$, as shown in Eq. 10.

$$\begin{gathered} w \sim N(0, \boldsymbol{Q}) \\ v \sim N(0, \boldsymbol{R}) \end{gathered} \tag{10}$$

Non-linear Kalman filters, such as the Extended Kalman Filter (EKF) and the Unscented Kalman Filter (UKF), are used when the state transition or measurement functions are non-linear. The EKF approximates these functions by linearizing them, which may introduce significant errors and degrade performance (Ref. 13). In contrast, the UKF avoids linearization by using sigma points that represent the mean and covariance of the state. These points are propagated through the non-linear functions to compute transformed state estimates and covariances (Ref. 14).

4.2. Filter state and model

Both fiducial markers and radio beacons algorithms give information about the two vehicles in relation to each other. The AHRS, instead, supplies data about the absolute state of the UAV. In absence of the GPS, the integration of accelerations leads to a drift of AHRS data. After these considerations, it seems more reasonable to track the relative state between UAV and ship instead of deriving the absolute states. However, since the UAV absolute linear velocities and angular rates are provided by the AHRS, it is possible to include the absolute TDP velocities in the filter state to employ a constant velocity process model with white Gaussian noise induced on the velocity terms (Ref. 4). It is important to keep in mind that the filter state does not correspond to relative state delivered to the flight control system, as described in section 4.3. The implications of such difference are important when the drift of the AHRS is introduced. The UKF state is defined as shown in Eq. 11.

$$\boldsymbol{x} = [\boldsymbol{x}_{HT}^\top, \dot{\boldsymbol{x}}_{WT}^\top, \boldsymbol{\Omega}_{HT}^\top]^\top = [x_{HT}, y_{HT}, z_{HT}, \dot{x}_{WT}, \dot{y}_{WT}, \dot{z}_{WT}, \varphi_{HT}, \theta_{HT}, \psi_{HT}]^\top \tag{11}$$

It is important to note that TDP velocities are variables that cannot be directly observed, therefore they must be determined through state updates when new measured relative positions are available. In addition, the real ship motion violates the hypothesis of gaussian white noise; however, the assumption that the ship velocity keeps constant can be a good approximation if camera data is provided at a sufficiently high frequency. In fact, with a high rate of updates, the filter can capture the changes of TDP velocity caused by the waves with a small tracking lag, which is an intrinsic drawback of the Kalman Filter algorithm, as discussed in Ref. 15. The relative orientation propagation model also neglects the ship motion with the assumption of null ship angular rates.

The state transition function is represented by Eq. 12; it allows to predict the $(k+1)^{th}$ filter state, given the k^{th} state and the current AHRS data.

$$\begin{aligned} \boldsymbol{x}_{HT,k+1} &= \boldsymbol{x}_{HT,k} + \boldsymbol{V}_{HT,k}\Delta t \\ \boldsymbol{V}_{WT_{k+1}} &= \boldsymbol{V}_{WT,k} \\ \boldsymbol{\Omega}_{HT,k+1} &= \boldsymbol{\Omega}_{HT,k} - \boldsymbol{L}_k^{-1}\boldsymbol{\omega}_{HH,k}\Delta t \end{aligned} \tag{12}$$

The relative velocity V_{HT} is defined below, in Eq. 13.

$$\boldsymbol{V}_{HT} = \boldsymbol{R}_{WH}^\top(\boldsymbol{V}_{WT} - \boldsymbol{V}_{WH}) - \boldsymbol{\omega}_{HH} \times \boldsymbol{x}_{HT} \tag{13}$$

The matrices $\boldsymbol{R}_{WH,k}^{T}$ and $\boldsymbol{L}_k^{-1}$ depend on the current UAV attitude. In particular:

- $\boldsymbol{R}_{WH}$ is a rotation matrix from NED frame to UAV frame, according to the Tait-Bryan 321 order (Ref. 16).
- $\boldsymbol{L}^{-1}$ represents kinematic equations needed to compute the derivatives of Euler angles from angular body velocities, as shown in Eq. 14.

$$\boldsymbol{L}^{-1} = \begin{bmatrix} 1 & \sin(\varphi)\tan(\theta) & \cos(\varphi)\tan(\theta) \\ 0 & \cos(\varphi) & -\sin(\varphi) \\ 0 & \sin(\varphi)/\cos(\theta) & \cos(\varphi)/\cos(\theta) \end{bmatrix} \tag{14}$$

Eq. 15 shows the measurement function which links the state variables to the Fiducial markers pose estimation, where $\boldsymbol{I}$ and $\boldsymbol{0}$ represent identity and null matrix respectively.

$$\boldsymbol{z}_{markers} = \begin{bmatrix} \boldsymbol{I}^{3\times3} & \boldsymbol{0}^{3\times3} & \boldsymbol{0}^{3\times3} \\ \boldsymbol{0}^{3\times3} & \boldsymbol{0}^{3\times3} & \boldsymbol{0}^{3\times3} \\ \boldsymbol{0}^{3\times3} & \boldsymbol{0}^{3\times3} & \boldsymbol{I}^{3\times3} \end{bmatrix} \boldsymbol{x} \tag{15}$$

When both fiducial markers pose estimation and radio beacons DOA estimation are available, the UKF employs Eq. 5 - 6 in addition to Eq. 15 to link the state to the measurements and to perform a single update.

The reason why beacons data is only used together with the camera pose estimation and not as an independent measurement lays behind the observability of the state vector, which cannot be guaranteed by the directions of arrival on their own.

The prediction step occurs at the frequency of AHRS, whose measurements are input of the state propagation model. The update step occurs when a valid pose estimation is computed from camera images and it can include data from radio beacons, if available. Table 4 shows the sensor frequencies.

Table 4: sensor frequencies.

Sensor	Frequency [Hz]
AHRS	50
Camera	20
Beacons	10

4.3. Filter response to the drift

The UKF can estimate the TDP absolute velocity combining the relative position information from the markers with that of the UAV state coming from AHRS. Since the fiducial markers estimation is not affected by any drift, the result of the expression in Eq. 13, defining the relative body velocity, shall converge to the true value. That expression contains the drifted UAV NED velocities, other AHRS measurements and the TDP absolute velocity. Thus, TDP velocities are updated by the filter so that the overall relative body position keeps approximately correct. The result is that TDP velocities are subjected to the same drift as that of the UAV velocities, but the relative velocity estimation delivered to the control system keeps unaffected.

5. RESULTS

5.1. Simulation results

Results in Figures 7 - 9 show the UKF state estimation compared to the ground truth and fiducial markers raw data, in the case of no AHRS drift. The chosen markers setup guarantees accurate estimations available from roughly 40 meters from the TDP. The additional sensor measurements employed to enhance the state estimation in the UKF are proven to bring the following improvements:

- Camera estimation noise reduction.
- Camera estimation bias reduction, obtained thanks to the radio beacons estimation.
- Velocity estimation.

Figure 8 shows the filter is capable of capturing, through indirect observations, the changes of velocity induced by the wave motion, introducing restrained noise and delay. A low latency is particularly important in the vertical velocity, as it allows the rotorcraft to set the vertical speed for the touchdown according to the structural limits, avoiding a too heavy impact with the ship deck.

As shown in Figure 9, the pose estimation with fiducial markers can be affected by non-zero-mean errors. The plot also shows that the filter can eliminate the bias by updating the state with radio beacons data. In fact, the combination of only camera and AHRS would not compensate for systematic errors introduced by the computer vision algorithm. Thus, the information regarding the degrees of arrival provided by radio beacons is proven to be useful for the state estimation improvement.

Table 5 shows the mean errors of state variables, comparing those of the UKF state and those of the fiducial markers' raw estimations. It is evident that the Kalman Filter improves the relative pose information provided by the camera and, in addition, allows for a velocity estimation whose accuracy is enough to perform a landing on the moving ship deck.

Table 5: mean errors of UKF state and markers estimation.

	Fiducial Markers	UKF
Relative position	0.20 m	0.13 m
TDP velocity	/	0.15 m/s
Relative orientation	0.7 deg	0.3 deg

When AHRS velocity is subjected to a drift, position and angular estimations do not undergo any worsening, while the ship velocity gets affected by the input error, as shown in Figure 10. As described in section 4.3, it is noticeable how the AHRS error in velocity components, starting from 1 m/s, is transferred to the TDP velocity estimation. However, as shown in Figures 11 - 12, the relative position and velocities in the NEU frame delivered to the FCS are not influenced by the drift.

6. CONCLUSIONS AND FUTURE DEVELOPMENTS

The aim of this research was to develop a navigation architecture for the automatic landing of a UAV on a ship-deck in a data link or GPS loss scenario and understand the potential of the selected sensor setup and algorithm, based on the fusion of computer vision, radio beacons, and inertial data.

For this purpose, the following tasks have been carried out:

- Development of a pose estimation algorithm based on the detection of fiducial markers.
- Real time simulation of radio beacons measurements based on real test data.

- Development of software infrastructure for the interconnection of the navigation algorithm with the guidance, control, and dynamics software.
- Modeling of a sensor fusion algorithm through an Unscented Kalman Filter.

Results obtained in this study led to key findings about the feasibility and effectiveness of the proposed architecture.

Fiducial markers proved to be an optimal tool to estimate the relative pose using the camera. The performance of the computer vision algorithm can be remarkably affected by light conditions and errors in the markers' mounting. In fact, small errors in the detection of the markers' corners can lead to big errors in the estimation of angles, which can worsen the position estimation significantly if the origin of the markers reference frame is distant from the surface of the markers, as in this case study. For this reason, pairing camera and radio beacons data is a good strategy for reducing the noise, filtering outliers and correcting systematic errors.

Results show that the sensor fusion algorithm performs well, given the sensor setup and formulation presented in this paper. For this reason, this research will undergo further advancements with real scaled flight tests, starting from data recording of a landing of a small drone on a moving platform. Flight tests will consolidate the validity of the algorithm, testing how it performs with reals sensors and environment. In addition, it would allow to assess the performance of the sensors and collect more data to improve sensor models

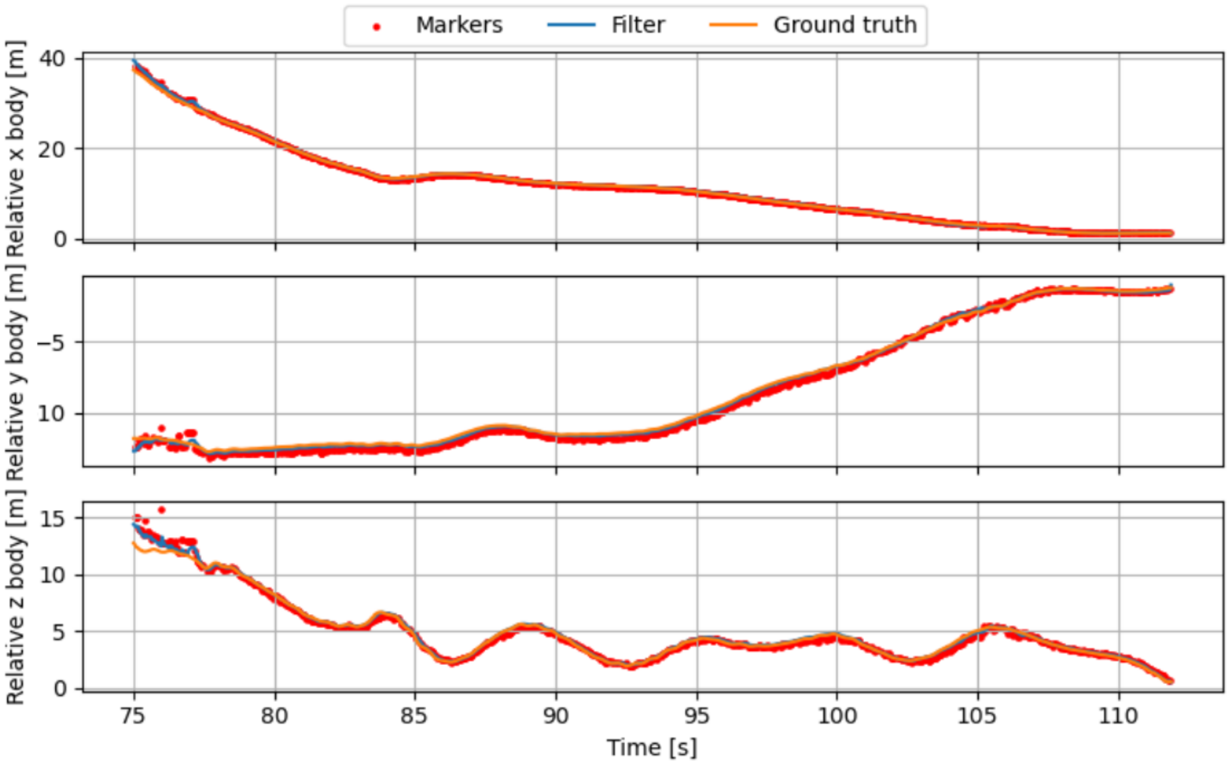

Figure 7: Fiducial markers and Kalman Filter relative body position estimation performance.

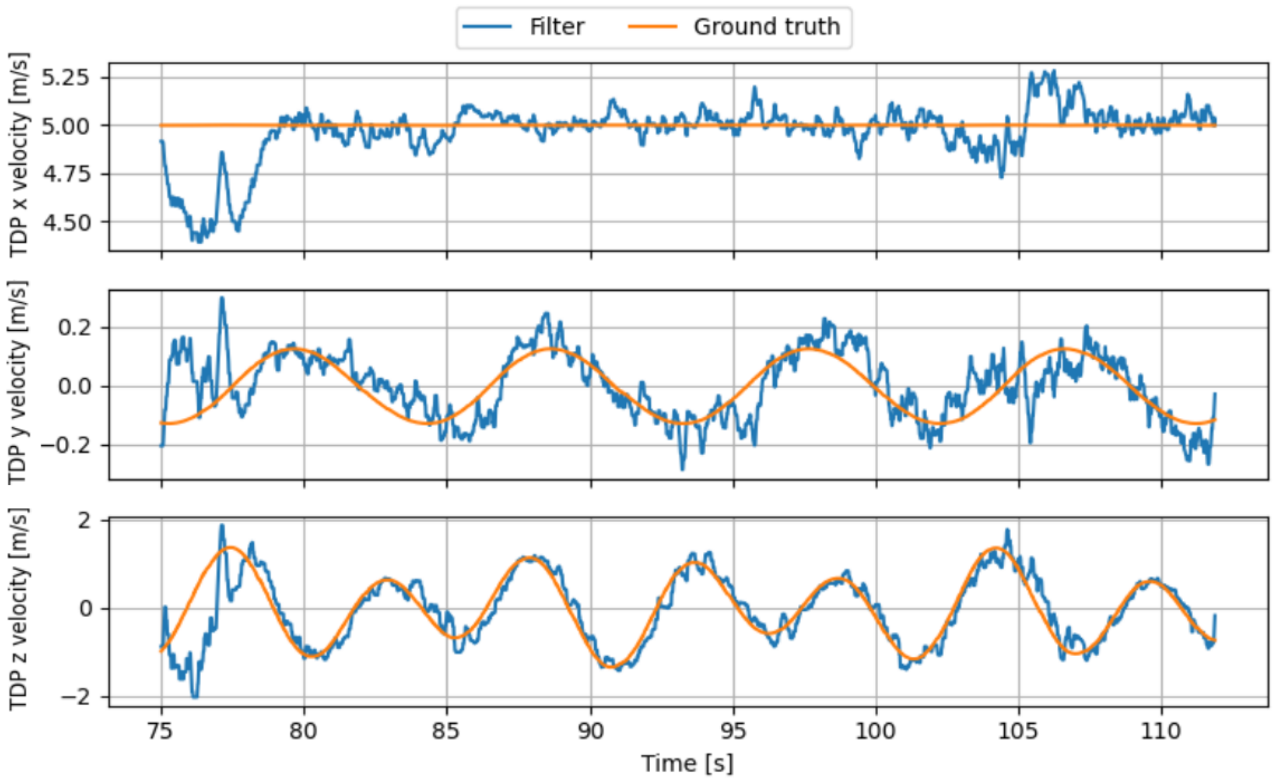

Figure 8: Kalman Filter TDP velocity estimation.

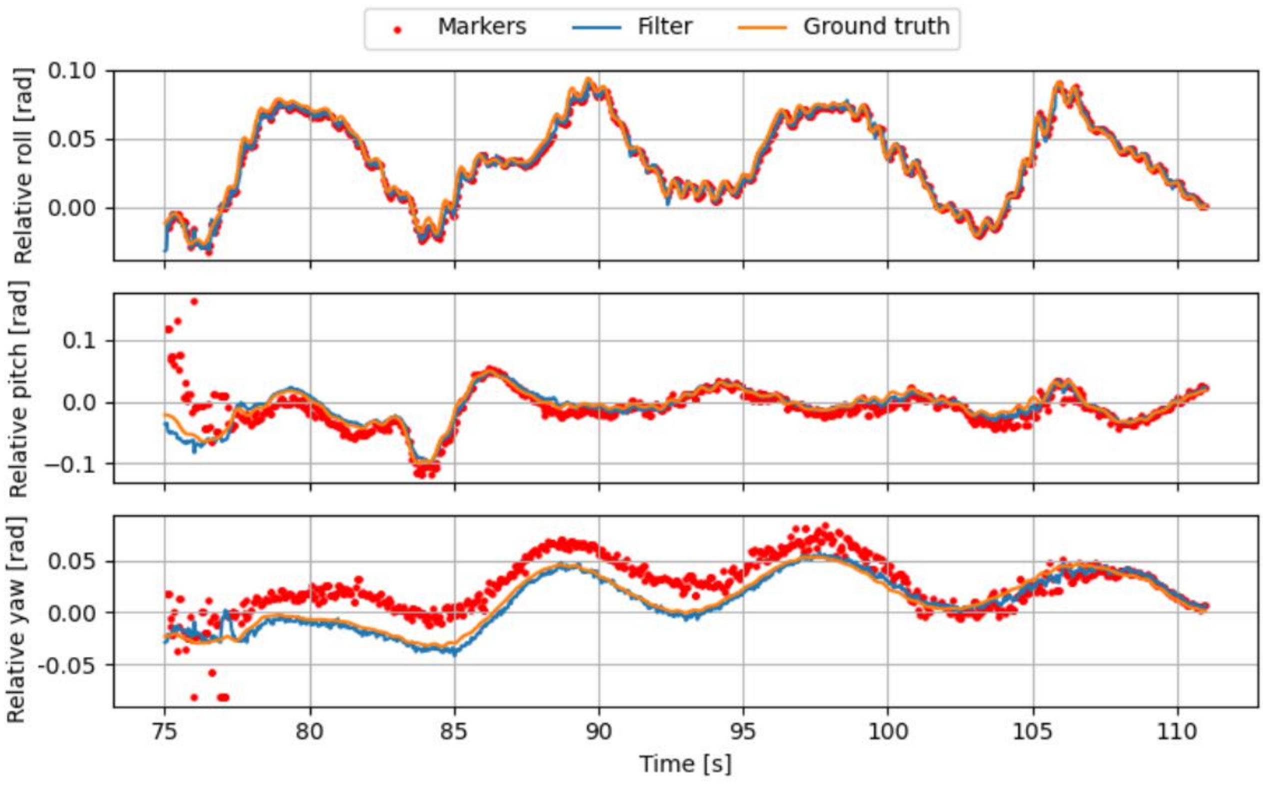

Figure 9: Fiducial markers and Kalman Filter Euler angles estimation.

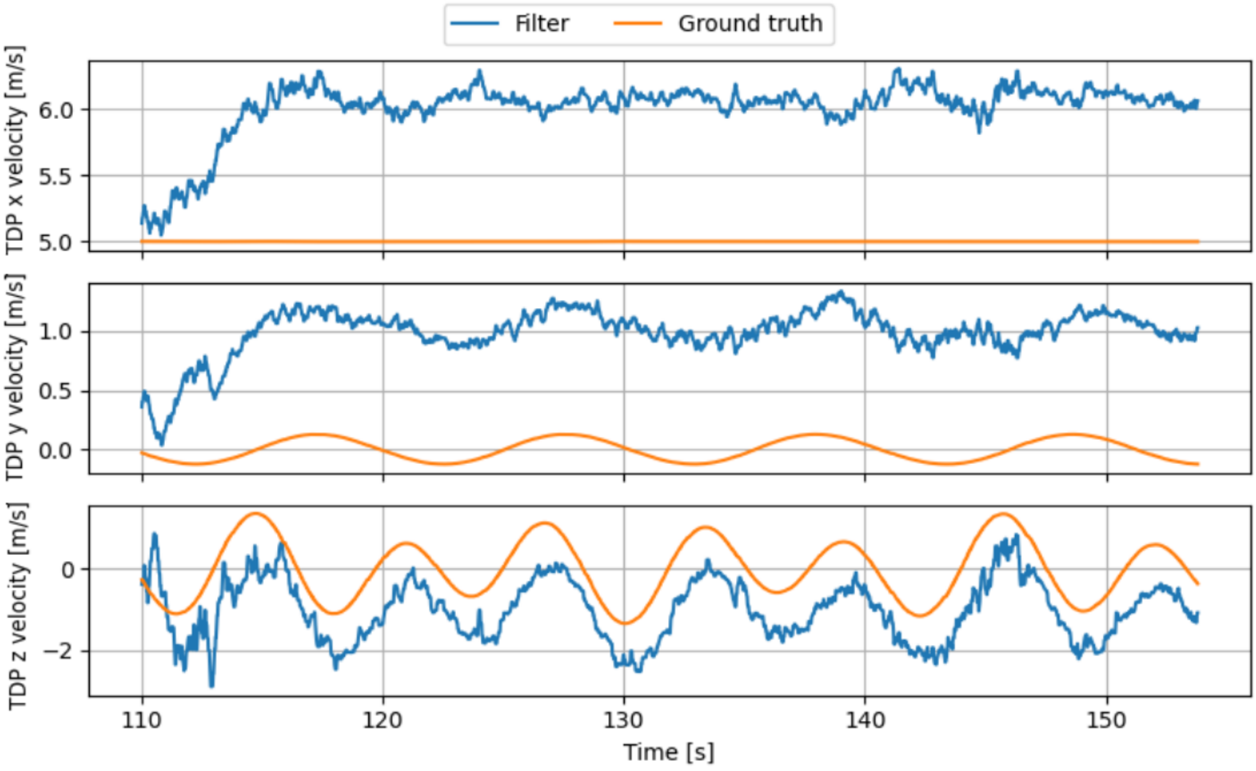

Figure 10: TDP velocity estimation with drift induced by AHRS. Initial drift value of 1 m/s in all UAV NED velocity components.

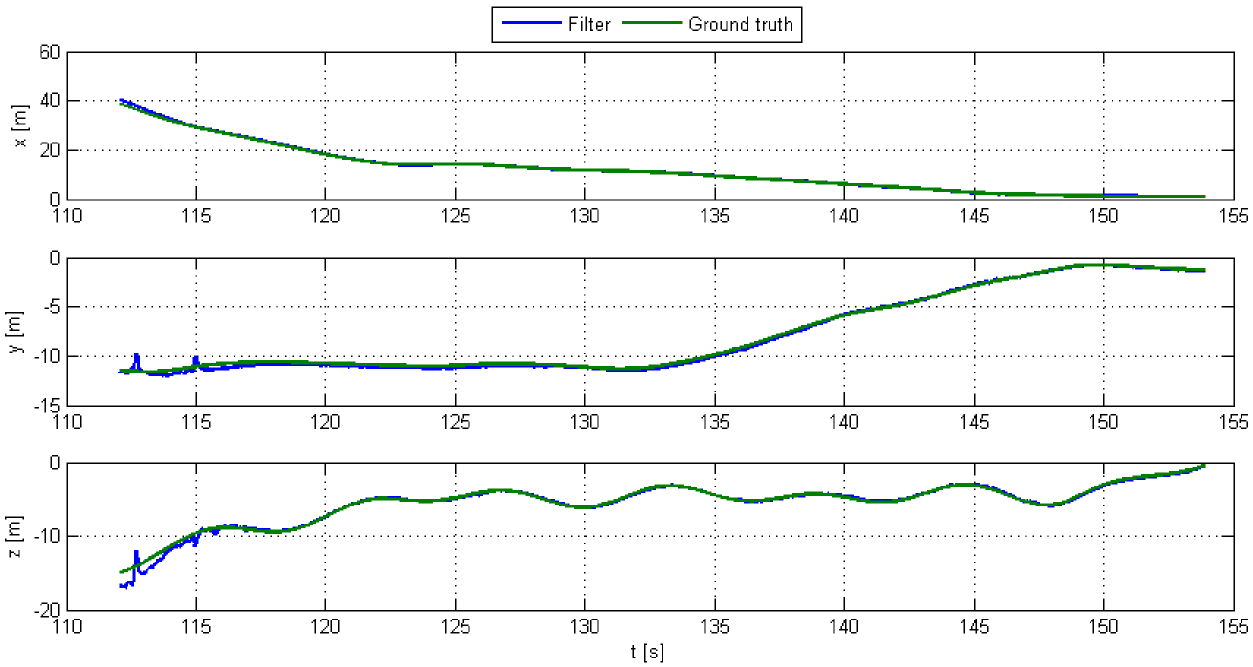

Figure 11: NEU relative position estimation in case of GPS loss, input to FCS. Initial AHRS velocity drift of 1 m/s on each velocity component.

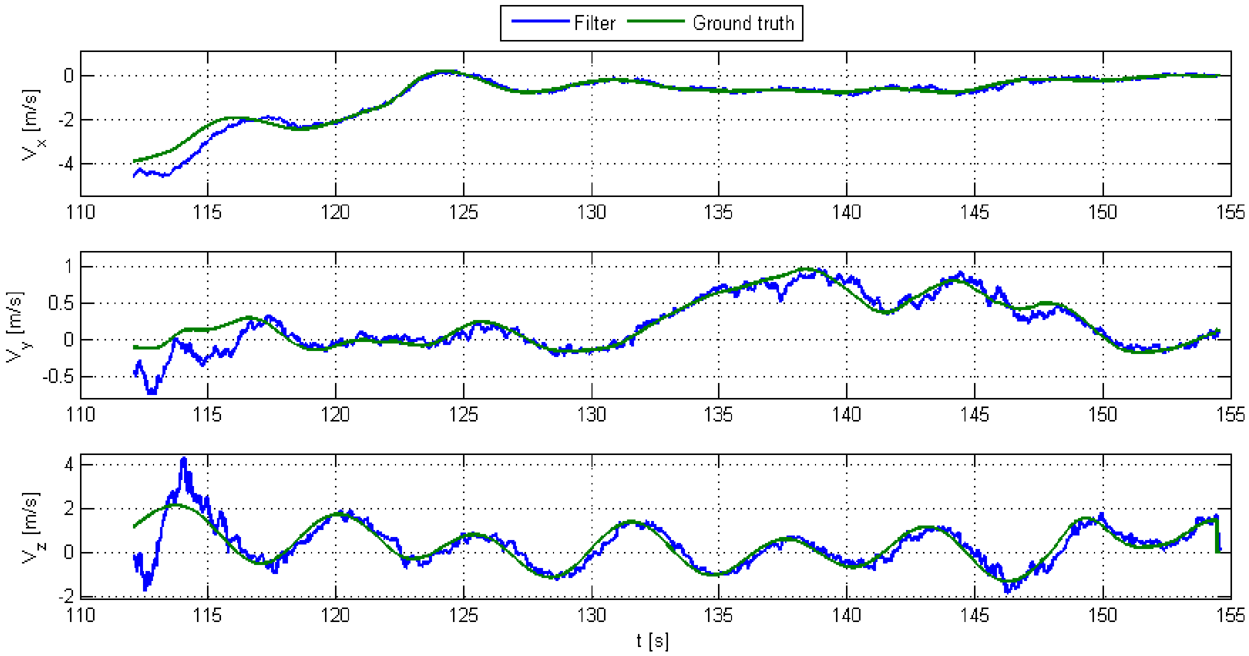

Figure 12: NEU relative velocity estimation in case of GPS loss, input to FCS. Initial AHRS velocity drift of 1 m/s on each velocity component.

7. REFERENCES

1. Wu, A., Johnson E., and Proctor, A., "Vision-Aided Inertial Navigation for Flight Control," *AIAA Guidance, Navigation, and Control Conference and Exhibit,* San Francisco, California, August 2005, pp. 15 – 18.

2. Kalaitzakis, M., Cain, B., Carroll. "Fiducial Markers for Pose Estimation." *Journal of Intelligent & Robotic Systems*, Vol. 101, (71), 2021, DOI: 10.1007/S.10864.020.01307-9.

3. Truskin, B. L., and Langelaan, J. W., "Vision-based Deck State Estimation for Autonomous Ship-board Landing," The Pennsylvania State University, Aerospace Department, 2013. 3

4. Chaves, S. M., Wolcott, R. W., and Eustice, R. M., "NEEC research: Toward GPS-denied landing of unmanned aerial vehicles on ships at sea," *Naval Engineers Journal*, Vol. 127, (1), 2015, pp. 23-35.

5. Jun D., Songlin, L., Hao, X., Zongbin, R., Xiao, Y., and Yunzhu, L. "Unmanned ground vehicle-unmanned aerial vehicle relative navigation robust adaptive localization algorithm," *IET Science, Measurement & Technology* Volume, Vol. 17, (5), January 2023, pp. 83-220, DOI: 10:1049/SMT2.12141.

6. ANSYS, Inc., "AVxcelerate Sensors Simulation Overview," Ansys AVxcelrate datasheet, 2022.

7. Piazzoni, A., Vijay, R., Cherian, J., Chen, L., and Dauwels, J., "Challenges in Virtual Testing of Autonomous Vehicles," *2022 17th International Conference on Control, Automation, Robotics and Vision (ICARCV)*, Singapore, Singapore, 2022, pp. 416-421, DOI: 10.109/ICARCV57592.2022.10004249.

8. St-Onge, D., and Herath, D. "The Robot Operating System (ROS1 &2): Programming Paradigms and Deployment," *Foundations of Robotics,* Springer, Singapore, September 2022, DOI: 10.1007/978-981-19-1983-1_5. 8

9. Probe, A., Oyake, A., Chambers, S. W., Deans, M., Brat, G., Cramer, N. B., Hambuchen, K. "Space ROS: An open-source framework for space robotics and flight software," *AIAA SCITECH 2023 Forum* (p. 2709).

10. Isaksson, J., and Magnusson, L., "Camera pose estimation with moving Aruco-board," Jönköping University, 2020.

11. Romero-Ramirez, F. J., Muñoz-Salinas, R., and Medina-Carnicer, R., "Speeded up

detection of squared fiducial markers," Image Vis. Comput. 76, 2018.

12. Grocholsky, B., DeFranco, P., Cover, H., Singh, A., and Singh, S., "Robust autonomous ship deck landing for rotorcraft." In *Proc. AHS 72nd Annu. Forum*, May 2016, pp. 1-4.

13. Wan, E. A., and Van der Merwe, R., "The Unscented Kalman Filter for Nonlinear Estimation," Oregon Graduate Institute of Science and Technology 20000 NW Walker Rd, Beaverton, Oregon 97006, 2000.

14. The MathWorks Inc. "Extended and Unscented Kalman Filter algorithms for online state estimation," MathWorks Documentation, 2023.

15. Tarvainen, M. P., Hiltunen, J. K., Ranta-aho, P. O., and Karjalainen, P. A., "Estimation of nonstationary EEG with Kalman smoother approach: an application to event-related synchronization (ERS)," *IEEE Transactions on Biomedical Engineering*, Vol. 51, (3), March 2004, pp. 516-524, DOI: 10.1109/TBME.2003.821029.

16. Henderson, D. M., "Euler angles, quaternions, and transformation matrices for space shuttle analysis," 1977.